2.B

*Nuclear Physics* **71** (1965) 353—372; 

# MEASUREMENTS OF d, pγ DIRECTIONAL CORRELATIONS IN $^{20}$F

ROSS W. NEWSOME, Jr. †

*Physics Department, University of Michigan* ††,
*Ann Arbor, Michigan, USA*

Received 25 February 1965

**Abstract:** The reaction $^{19}$F(d, pγ)$^{20}$F was used to measure the directional correlations of the proton groups in coincidence with subsequent gamma radiations produced in de-excitation of the 2.05, 1.31, 1.06, 0.99 and 0.65 MeV levels of $^{20}$F. The effective deuteron energy was 0.448 MeV. For the 2.05 MeV level, the 1–2 correlation between the protons and the 1.40 MeV gamma transition to the first excited state was measured simultaneously with the 1–3 correlation between the same proton energy group and the 0.65 MeV gamma transition, with the intermediate 1.40 MeV gamma radiation unobserved. These correlations were measured in two configurations: one with the protons being detected at an average angle of 170° with the beam passing through a centre hole in an annular-shaped detector, and the other with a disc-shaped detector at 135° and the gamma detector moving in the plane of the reaction. A plane-wave analysis of these data gave essentially identical correlation coefficients for these two configurations.

Directional correlations were also measured in the 170° configuration between the proton energy groups and the subsequent ground-state gamma transitions from the 1.31, 1.06, 0.99 and 0.65 MeV levels. A plane-wave analysis of these data is compared with a distorted-wave analysis of related data from a previous experiment. A thorough computational comparison between all of these data and the predicted correlations, based on a plane-wave analysis using postulated spin values which are consistent with the proton angular distribution data, did not yield a unique spin value for any of these levels. It was possible in some cases, however, to put rather stringent conditions on the ratios of the angular-momentum matrix elements associated with the incoming and outgoing radiations which are compatible with the postulated spins.

E NUCLEAR REACTIONS. $^{19}$F(d, pγ), $E$ = 0.448 MeV; measured $\sigma(E_p)$, pγ-coin, pγ(θ).

## 1. Introduction

Measurement of the spins of the various low-lying excited states of $^{20}$F could conceivably provide a useful check of the theoretical models formulated for this nucleus [1, 2]). Measurements of the proton angular distributions from the reaction $^{19}$F(d, p)$^{20}$F have contributed significantly toward this goal. Such measurements have recently been re-investigated by many authors [3–5]), and they cover an extended incident deuteron energy range which goes as low as 800 keV. Their results for the angular-momentum transfer ($l$) for the low-lying states in $^{20}$F are in good agreement,

† Now at Los Alamos Scientific Laboratory, Los Alamos, New Mexico.

†† This work was supported by the U.S. Atomic Energy Commission.

and in most cases uniquely establish the parity and limit the spin to one of three possible values.

Recently the d, p$\gamma$-directional correlations involving four of the low-lying states in $^{20}$F were measured by Chagnon [6]) in three orthogonal planes, and the resultant data were analysed using the distorted-wave Born-approximation [7]). This work resulted in a unique spin assignment for the 1.31 MeV level, but did not limit the choice of the spins for the first excited state at 0.65 MeV. One of the primary purposes of the present work was to investigate the possibility of determining the spin of this 0.65 MeV state via measurements of the 1–2 and 1–3 p-$\gamma$ directional correlations which proceed from the 2.05 MeV level. The 1–2 correlation involves detection of the 1.4 MeV gamma radiation, while for the 1–3 correlation the subsequent 0.65 MeV gamma radiation is detected and the intermediate 1.4 MeV gamma radiation is unobserved. The analysis of the data was greatly simplified by assuming that the plane-wave approximation is valid when the protons are detected along the beam direction [8, 9]). The question as to the validity of this assumption for this particular nucleus is discussed in greater detail in sect. 5. As an added check, the correlations measured by Chagnon were repeated in order to see if his results could be verified using this simplified experimental and analytical approach.

## 2. Experimental Method

A beam of 470 keV deuterons from a Van de Graaff accelerator was used to bombard thick $CaF_2$ targets which had been vacuum-evaporated onto copper backings. A yield-versus-energy measurement [6]) for the reaction $^{19}$F(d, p)$^{20}$F showed that the effective beam energy was 448 keV. A typical beam current of approximately 4.5 $\mu$A on the target was found to give the best compromise between counting rate losses and the accumulation of relevant data. A positive voltage of approximately 50 V was applied to the target in order to suppress secondary electron emission.

For the work on the 2.05 MeV level, the beam was collimated to a diameter of 5 mm. The copper target backing was 0.55 mm thick and could be moved vertically to five fresh positions without opening the vacuum chamber. For detection of the protons at 135°, a circular disc-shaped Ortec surface-barrier detector with a sensitive area of 300 mm$^2$ was used. The target was 3 cm from the sensitive surface of the detector and was oriented parallel to this surface. For detection of the protons in the extreme backward direction, a similar Ortec detector was used which had an 8 mm diam. centre hole through which the beam passed. The perpendicular distance between the sensitive surface and the target was 4 cm. Due to the eventual failure of this detector, it was replaced for the work on the lower energy levels of $^{20}$F by a similar Ortec detector with a 4 mm diam. centre hole. The beam was then collimated to a diameter of 3 mm, and the sensitive-surface to target distance was reduced to 2.5 cm. For this latter work, the thickness of the copper backing was reduced to 0.13 mm in order to reduce gamma-ray absorption. The $CaF_2$ was vacuum-evaporated onto both

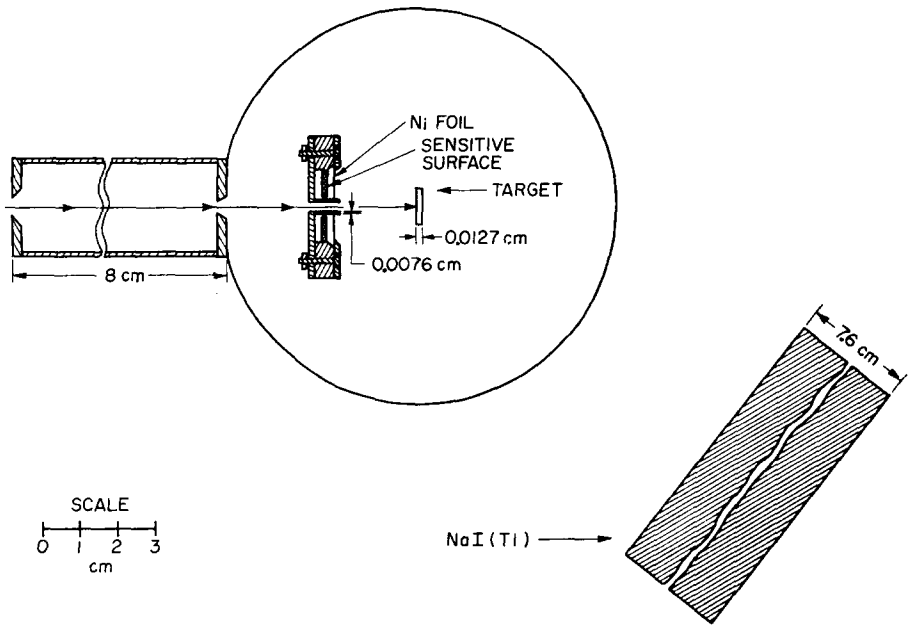


Fig. 1. A schematic drawing of a typical experimental arrangement. The beam enters from the left and passes through the centre hole in the angular detector. The NaI(Tl) detector moves in the plane of the drawing.

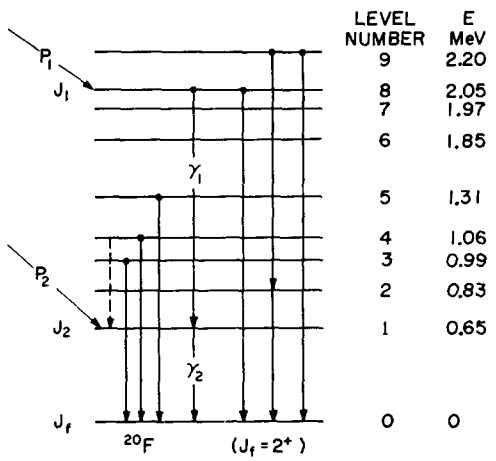


Fig. 2. A decay scheme of the prominent gamma-transitions [6]) from the low-lying states in $^{20}$F. The proton groups associated with d, p stripping to the 2.05 and the 0.65 MeV levels are symbolically indicated by $P_1$ and $P_2$.

sides of these backings. This provided 14 fresh target positions without opening the target vacuum chamber. A drawing of this latter experimental arrangement is shown in fig. 1.

The various solid-state detectors were operated at voltages such that 4.4 MeV protons would be stopped in their depletion layers. A nickel foil 2.3 mg/cm$^2$ thick was used to prevent elastically scattered deuterons from entering the detectors. With this foil in place, the typical energy resolution was approximately 180 keV (i.e. full width at half maximum).

The gamma radiation was detected in a cylindrical NaI(Tl) crystal, 7.6 cm × 7.6 cm, which was integrally mounted to a Dumont 6363 phototube. This detector moved in the horizontal centre plane, and its angular range of positions varied from 0° to 135° on both sides of the beam direction. The data were collected with the angular positions of this detector spaced at 15° intervals. The sequence of angular positions was randomized, and a fresh region of the target was exposed each time the angle was changed. The length of time spent at each angular position was typically 40 min.

There was a marked increase in the gamma singles rate when the gamma detector was moved to angles greater than 105°. This increase was primarily due to background radiation from the beam collimators. The effect of this radiation on the coincidence rate was almost negligible, however, because this background gamma radiation was not in coincidence with any charged particles in the energy range of interest, and also because the chance-coincidence rate was no more than 10 % of the true rate for the most unfavourable proton-gamma cascade.

The relative gamma-ray absorption was measured as a function of angle at the end of each series of runs. This was done by covering the target area, which had been burned by the beam, with a radioactive source which emitted gamma radiation of approximately the same energy as that under investigation. The relative singles counting-rate as a function of angle yielded the gamma-absorption factor directly. For the work involving the 2.05 MeV level, this correction was typically 7 %, and for the latter work on the lower energy levels it was never more than 4 %.

The electronic network was essentially a fast-slow coincidence arrangement which was used to gate a Nuclear Data Model 150 FM two-parameter analyser. A set of linear microsecond gates [10]) was used to reduce dead time losses and pile up in the slow part of the coincidence logic. The fast-coincidence circuit was set at a resolving time $2\tau$ of 60 m$\mu$sec. The contribution to the chance rate from first-order effects was periodically monitored by inserting a sufficiently long delay in one of the inputs to the fast-coincidence unit. As mentioned previously, the largest chance contribution was only 10 % of the true rate, and therefore higher-order accidental rate effects were neglected.

An Ortec Model 101 preamplifier was used with the solid state detectors. The output pulse for the fast-coincidence circuit, which was taken from an early stage of this preamplifier, had a rise time of approximately 60m$\mu$sec. The slow output of this preamplifier was fed to a differential discriminator which was used to monitor the high-

energy alpha-group (approximately 8 MeV) from the ground-state transition in the reaction $^{19}F(d, \alpha)^{17}O$. The yield-versus-energy curve of this alpha group is similar to that of the proton groups of interest [6]), and therefore the coincidence rates obtained at the various angular positions of the gamma detector were normalized with this reference singles rate.

## 3. Experimental Results

A gamma-decay scheme [6]) of the relevant levels in $^{20}F$ is shown in fig. 2. A typical singles spectrum, taken with one of the annular solid-state detectors, is shown in fig. 3. This spectrum was obtained with a mean proton angle of approximately 170°

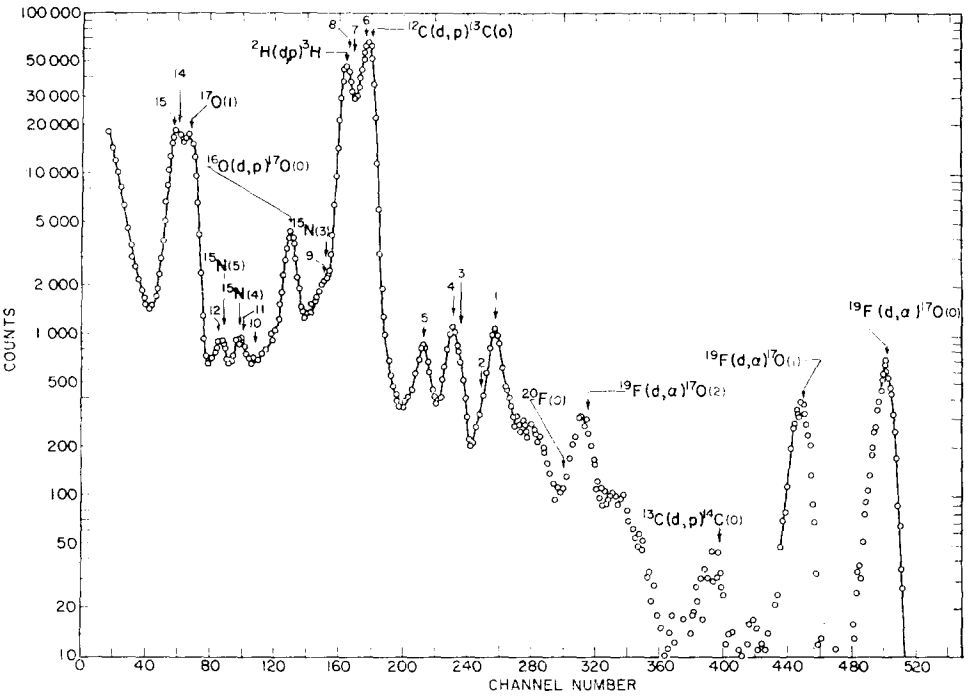


Fig. 3. A typical charged-particle singles spectrum taken with an annular-shaped detector. The lone Arabic numbers refer to the levels in $^{20}F$ which are listed in fig. 2.

and an effective deuteron energy of 448 keV. The excited states in $^{20}F$ are indicated by the lone arabic numbers, and the corresponding excitation energies are listed in fig. 2. Identification of the various peaks was made by requiring that a plot of channel number versus energy fall on a straight line. The energy was obtained from the kinematics of a given reaction and was corrected for absorption in the nickel foil shield [11]). The gamma singles spectrum was even more congested, and it possessed very few distinct peaks. Fortunately the coincidence spectrum was relatively unambiguous.

This is demonstrated in fig. 4 for the proton group which feeds the 2.05 MeV level. For convenience of presentation, the spectra in fig. 4 were obtained from the two-parameter analyser output by summing the rows and columns which respectively show the coincidence gamma-ray and proton profiles. The data for these plots were taken from a typical 40 min run. De-excitation of the 2.05 MeV level is predominantly a two-step cascade. A 1.4 MeV gamma transition to the first excited state is followed

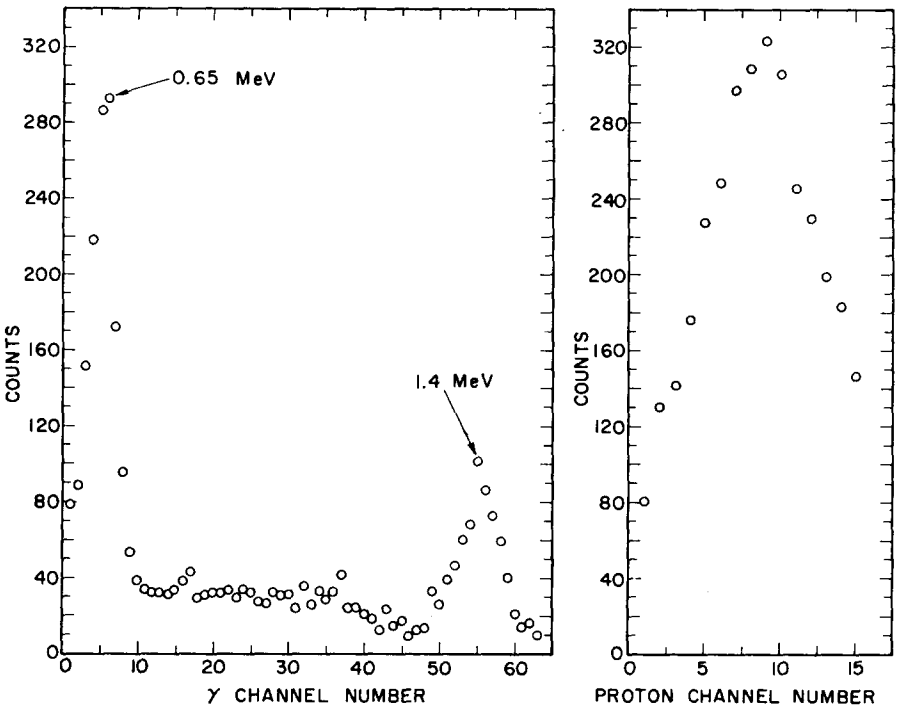


Fig. 4. The gamma-ray and proton coincidence profiles of the 2.05 MeV level. These data were taken from a typical run with the two-parameter analyser.

by the 0.65 MeV gamma transition to the ground state. The 1.4 and 0.65 MeV gamma peaks therefore respectively represent the 1–2 and 1–3 coincidence cascades with the proton group which feeds the 2.05 MeV level. The 0.65 MeV photopeak was corrected for contributions from the 1.4 MeV Compton distribution by extrapolation of this relatively flat distribution under the 0.65 MeV photopeak.

It was possible to resolve the proton group to the 2.20 MeV state from the group to the 2.05 MeV state. The 1.97 MeV level, however, could not be resolved. Recent high-resolution proton angular-distribution work [3,4]) indicates the relative yield of the 2.05 to the 1.97 MeV levels, in the angular and energy ranges of interest, is greater than six to one. Possible contributions from the 1.97 MeV level were therefore neglected, but any refinement of the present work would certainly require a closer examination of contributions from this level.

In fig. 5 the 1–2 and 1–3 directional correlation data are respectively presented for the 1.4 and the 0.65 MeV gamma rays. These data were taken simultaneously with the disc-shaped particle detector at 135°. Data were obtained at most of the angular positions of the gamma detector for at least four independent measurements, and the error flags represent the standard deviation from the mean of each set of such measure-

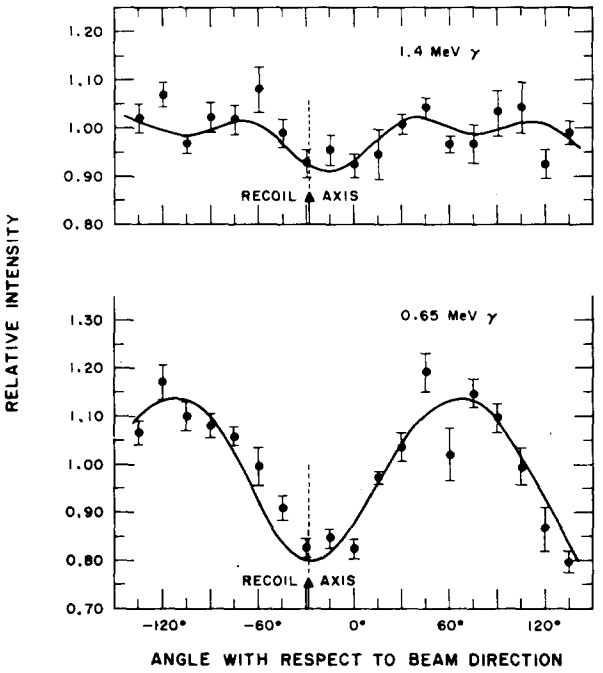


Fig. 5. The 1–2 and the 1–3 directional-correlation data, originating from the 2.05 MeV level, obtained via detection of the 1.4 and the 0.65 MeV γ-radiations, respectively. The proton detector was at 135°.

ments. The data in this figure have been corrected for the relative gamma absorption, but they have not been corrected for the finite solid angle subtended by the detectors. The solid curves represent a least-squares fit [12]) of the data points to the following trigonometric series:

$$W(\theta) = 1+\beta_1 \sin(2\theta)+\beta_2 \cos(2\theta)+\beta_3 \sin(4\theta)+\beta_4 \cos(4\theta). \qquad (3.1)$$

The position of the $^{20}$F recoil axis coincides, within the range of experimental accuracy, with the symmetry axes of the data in fig. 5. This is in agreement with the prediction of the plane-wave approximation.

These correlation measurements for the 1.4 and the 0.65 MeV γ-radiation were repeated with an annular-shaped proton detector which had an 8 mm diam. centre hole. The average angle subtended by this detector was approximately 170°. Due to the

axial symmetry of this proton detector about the beam axis, these data were averaged symmetrically about the beam direction as shown in fig. 6. The smooth curves through the data points in this figure represent least-squares fits to the first three even Legendre polynomials. A quantitative comparison between the extracted coefficients obtained using this Legendre-polynomial fit with the coefficients obtained from the previous

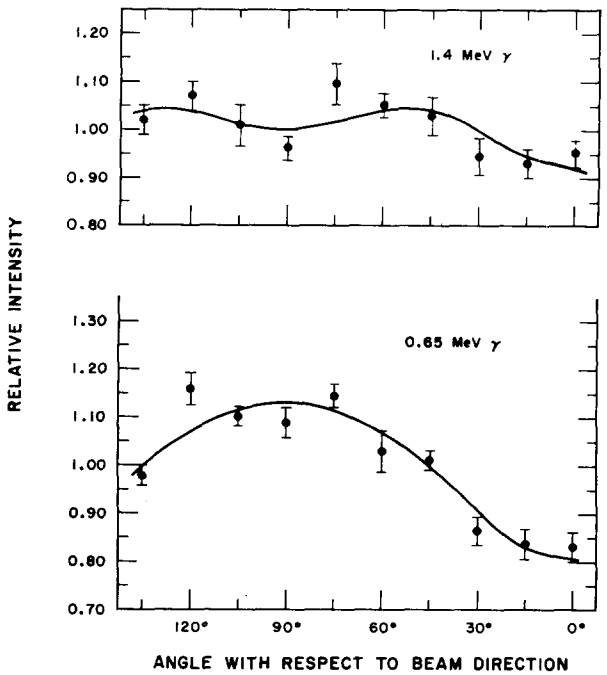


Fig. 6. The 1–2 and the 1–3 directional-correlation data for the 2.05 MeV level obtained via detection of the 1.4 and the 0.65 MeV $\gamma$-radiations, respectively. The mean angle subtended by the annular proton detector was approximately 170°.

sine-cosine fits to the 135° data can be obtained with the following generalized Legendre polynomials:

$$W(\theta) = 1 + A_2 P_2 \cos(\theta - \theta_2) + A_4 P_4 \cos(\theta - \theta_4). \tag{3.2}$$

The angles $\theta_2$ and $\theta_4$ represent the angular position of the symmetry axis, and they should be identical in the plane-wave approximation. By expressing eq. (3.2) in terms of sines and cosines, the coefficients $A_i$ and the symmetry angles $\theta_i$ may be related to the coefficients $\beta_j$ in eq. (3.1). A summary of the results obtained in this fashion is shown in table 1. Note that the entries in columns number 3 and 6 of table 1 refer to a least-squares sine-cosine fit of the 170° data before it was averaged about the beam direction.

The coefficients $A_i$ in table 1 were corrected for solid angle attenuation as described in the appendix. The coefficients obtained with either of the two proton-detector

angular configurations agree to within the calculated accuracy of the data. It follows that these results, obtained using the plane-wave approximation, are consistent over the angular range from 135° to 170°. This implies that distorted wave effects are either not resolved or are very slowly varying over this angular region.

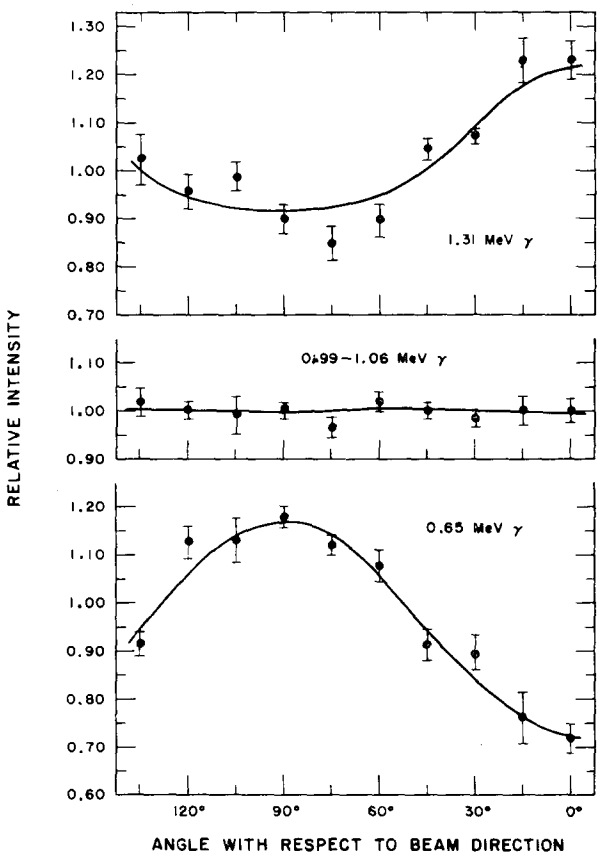


Fig. 7. The 1–2 directional-correlation data for the 1.31, 0.99–1.06, and the 0.65 MeV levels. The 0.99 and the 1.06 MeV γ-radiations were not resolved. The mean angle subtended by the annular proton detector was approximately 170°.

Proton groups to the 1.31, 1.06, 0.99 and 0.65 MeV levels in coincidence with the subsequent ground-state gamma transitions were also investigated. A scale drawing of this particular experimental arrangement is shown in fig. 1. These four coincidence groups were recorded simultaneously with the two-parameter analyser. The separation of the three main groups was excellent; however, it was impossible to resolve the 1.06 and 0.99 MeV levels. The Compton distributions down to 0.6 MeV were added to the 1.31 and 1.06–0.99 MeV photopeaks in order to improve the statistical accuracy. In handling the raw data, the photopeaks and Compton continua were summed

TABLE 1

Summary of the d, p$\gamma$ correlation coefficients and recoil angles obtained for the two p, $\gamma$ cascades associated with the 2.05 MeV level

| Gamma energy | 0.65 MeV (1–3 correlation) | | | 1.4 MeV (1–2 correlation) | | |
|---|---|---|---|---|---|---|
| Particle detector | Disc | Annular | Annular [a]) | Disc | Annular | Annular [a]) |
| Mean proton angle | 135° | 170° | 170° | 135° | 170° | 170° |
| $A_2$ | −0.251±0.036 | −0.240±0.035 | −0.215±0.029 | −0.056±0.031 | −0.035±0.037 | −0.027±0.029 |
| $A_4$ | −0.037±0.04 | −0.076±0.034 | −0.034±0.04 | −0.082±0.034 | −0.090±0.042 | −0.093±0.041 |
| $\theta_2$ | 25±4° | 3± 2° | | 18±10° | 10± 6° | |
| $\theta_4$ | 33±16° | 14±12° | | 15±12° | 15±10° | |

[a]) Assumed symmetry about the beam axis with a least-squares fit to the first three even Legendre polynomials

TABLE 2

A comparison of the extracted d, p$\gamma$ correlation coefficients obtained from the distorted wave analysis of Chagnon's data [6]) with the plane wave analysis of the present data

| Gamma energy | 0.65 MeV | | 0.99–1.06 MeV | | 1.31 MeV | |
|---|---|---|---|---|---|---|
| | Present work | Chagnon | Present work | Chagnon | Present work | Chagnon |
| $A_2 \to \eta_2 F_2$ | −0.330±0.025 | −0.291±0.02 | 0.0004±0.013 | ≈ 0 | 0.199±0.034 | 0.03±0.05 |
| $A_4 \to \eta_4 F_4$ | 0.007±0.039 | 0±0.03 | −0.015±0.02 | ≈ 0 | 0.086±0.062 | 0.17±0.07 |

separately, and they were combined when it became apparent that there was no significant statistical difference in their relative coincidence rates.

The directional correlation data for the 1.31, 0.99–1.06 and 0.65 MeV levels are presented in fig. 7. The data in this figure have been corrected for relative gamma-ray absorption, but not for solid angle effects. The error flags represent the standard deviations from the mean of the various runs at a given angle, and the solid curves were obtained from a least-squares fit to the first three even Legendre polynomials. In table 2 the extracted coefficients from the least-squares analysis are summarized and compared with the corresponding coefficients which Chagnon [6]) obtained. Note that in Chagnon's work, the directional correlations were measured in three orthogonal planes, and the coefficients $\eta_2 F_2$ were extracted with an analysis based on the distorted-wave Born approximation. The data in table 2 have been corrected for the finite solid angles subtended by the detectors.

## 4. Analysis of the Data

The most general form of the directional correlation function for the proton and gamma-ray resulting from a d, pγ nuclear reaction is [9])

$$W(\theta, \phi) = \sum_{kq} a_{kq} C_{kq}(\theta, \phi), \tag{4.1}$$

where the angles $(\theta, \varphi)$ define the direction of emission of the gamma-ray with respect to the proton direction in the centre-of-mass system, and the functions $C_{kq}(\theta, \varphi)$ represent the normalized spherical harmonics. If the stripping mechanism can be described in the distorted-wave Born approximation with a unique $l$ value (neglecting spin orbit coupling in the distorted waves), then the coefficients $a_{kq}$ may be expressed as

$$a_{kq} = g_k d_{kq}. \tag{4.2}$$

The dynamical factors $d_{kq}$ contain the matrix elements obtained from the distorted-wave Born approximation, and the factors $g_k$ contain the dependence on the nuclear spins and the total angular momentum $j = l \pm \frac{1}{2}$ of the captured neutron.

In the Butler plane-wave theory, eq. (4.1) reduces to

$$W(\theta) = \sum_{k} g_k P_k (\cos \theta), \tag{4.3}$$

where $P_k$ are the Legendre polynomials, and the reference axis has been chosen along the recoil direction of the residual nucleus. The geometrical factors $g_k$ may be expressed as:

$$g_k = \Big(\sum_{jj'} \theta_{jl} \theta_{j'l} \eta_k(jj' J_i J_1)\Big)\Big(\sum_{LL'} C_L C_{L'} F_k(LL' J_2 J_1)\Big), \tag{4.4}$$

where $J_i$ is the spin of the target nucleus, $J_1$ is the spin of the intermediate excited state, and $J_2$ is the spin of the subsequent state following gamma emission. The

reduced width for capture with $j = l \pm \frac{1}{2}$ is represented by $\theta_{jl}$, and $C_L$ is the reduced matrix element for $2^L$-pole gamma radiation. The factors $\eta_k$ and $F_k$ represent the relevant vector-addition coefficients. Eq. (4.4) is often written in the abbreviated notation $g_k = \eta_k F_k$. In general the lowest order electric and magnetic multipoles will dominate the gamma transition, and therefore the mixing ratio $\delta$ may be defined as $\delta = C_{L'}/C_L$. The corresponding fractional intensity $Q_G$ is defined as $Q_G(\delta) = \delta^2/(1+\delta^2)$. An analogous set of definitions will be utilized for the reduced widths $\theta_{jl}$.

Using the previously defined notation, the 1–3 directional correlation function which describes the relative coincidence rate between protons, from a d, p reaction with a unique $l$ value in the plane-wave approximation, and a subsequent double gamma cascade with the intermediate gamma ray unobserved, is given by

$$\begin{aligned} W(\theta) = \sum_{v} & \{\eta_v(jjJ_iJ_1)(1-Q_p)+2\eta_v(jj'J_iJ_1)(Q_p(1-Q_p))^{\frac{1}{2}} \\ & +\eta_v(j'j'J_iJ_1)Q_p\}\{(1-Q_{G1})G_{v0v}(L_1L_1J_2J_1)(2v+1)^{\frac{1}{2}} \\ & +Q_{G1}G_{v0v}(L_1'L_1'J_2J_1)(2v+1)^{\frac{1}{2}}\}\{(1-Q_{G2})F_v(L_2L_2J_fJ_2) \\ & +2(Q_{G2}(1-Q_{G2}))^{\frac{1}{2}}F_v(L_2L_2'J_fJ_2)+Q_{G2}F_v(L_2'L_2'J_fJ_2)\}P_v(\cos\theta). \quad (4.5) \end{aligned}$$

In this equation, the $z$-axis lies along the nuclear recoil direction, and only two distinct values of $j$ or $L$ are considered for each transition. The vector addition coefficients $G_{v0v}$, $\eta_v$, and $F_v$ are defined and tabulated by Rose [13]), Satchler [14]), and Ferentz and Rosenzweig [15]) respectively. A few discrepancies were found in the table of $G_{v0v}$ coefficients [13]). They were therefore independently calculated using a table of Racah coefficients [16]) and the formula [13])

$$G_{v0v}(LLJ'J) = \left[\frac{(2J+1)(2J'+1)}{(2v+1)}\right]^{\frac{1}{2}}(-1)^{L-J-J'}W(JJJ'J';vL), \quad (4.6)$$

where $W$ is the well-known Racah coefficient. Note that the formula corresponding to a 1–2 directional correlation can be obtained from eq. (4.5) by replacing the contents in the middle curly brackets by unity. Also note that the terms in each of these curly brackets have been normalized with the appropriate factor $1/(1+\delta^2)$.

From proton angular distribution work [3–5]), the relative parities of the relevant levels in $^{20}$F are known, and the spins are limited in most cases to values of either 1, 2 or 3. For $l = 2$ stripping of a spin-$\frac{1}{2}$ target, the total angular momentum $j$ of the captured neutron must be $\frac{3}{2}$ if the spin of the excited level is 1, and $\frac{5}{2}$ if the spin is 3. Both $j$ values can contribute to an excited state of spin 2.

The assignment of spin 2 for the ground state of $F^{20}$ rests almost completely on the results of two beta circularly-polarized gamma directional-correlation experiments [17, 18]). The formulae used to predict the circular polarization correlation functions associated with the three postulated spin values were based on the Konopinski-Uhlenbeck approximation. Although the accuracy of these predictions could undoubtedly be improved by using more exact expressions for the electron wave func-

tions [19]), there is good reason to believe that the Konopinski-Uhlenbeck approximation will be adequate for this beta transition if there are no severe cancellations of the nuclear matrix elements. This is because the end point energy of this beta transition from the ground state of $^{20}$F is large compared to the Coulomb energy of an electron at the nuclear surface; and therefore the Coulomb distortion of the electron wave function, which is very sensitive to the finite size of the nucleus, is probably negligible. The quoted value of 2 for the ground state spin of $^{20}$F was therefore assumed to be correct and was used for all the calculations in the present work.

The method used to select the most probable spins which were consistent with the d, pγ correlation data was to compare quantitatively this experimental data with the predictions of eq. (4.5) for a postulated spin sequence. The experimental data were of course first corrected for the finite solid angles subtended by the detectors as outlined in the appendix. A high-speed digital computer was used to calculate the predicted correlation coefficients as a function of the fractional intensity variables $Q$. The computer then used the sum of the $\chi^2$ values associated with the $A_2$ and $A_4$ coefficients as a quantitative indication of the applicability of a postulated spin sequence. The $\chi^2$ calculations were based on the equation

$$\chi^2 = \left[\frac{\text{theoretical prediction} - \text{experimental result}}{\text{experimental error}}\right]^2. \tag{4.7}$$

The fractional intensity $Q$ varies continuously from 0 to 1 and is always positive. However, the various sign combinations for the mixing ratios must be treated separately. This follows from the sign ambiguity associated with the square-root terms in eq. (4.5). These terms are explicitly related to the mixing ratio $\delta$ by the equation

$$\frac{\delta}{1+\delta^2} = \pm[Q(1-Q)]^{\frac{1}{2}}. \tag{4.8}$$

Specifically, the computer was instructed to consider all possible combinations of $Q$ values over the range from 0 to 1 and in intervals of 0.05. It was also instructed to consider all four possible sign combinations for the mixing ratios. The computer print-out consisted only of the various $Q$ value combinations which yielded $\chi^2$ values below a specified upper limit. These results were further classified by the computer into groups which had $\chi^2$ values within specified intervals. The solutions were thus grouped according to how well they predicted the experimental data. The total computation and print-out time for a complete analysis of a given spin sequence was normally less than one minute.

A quantitative summary of typical predictions, for the 1–3 and the 1–2 directional correlations involving the 2.05 and the 0.65 MeV levels, and their respective $\chi^2$ values for representative minima in the $\chi^2$ surfaces is given in table 3. It is apparent that only four of the possible nine spin combinations can be effectively eliminated. One of the possible sets of spin assignments which would be compatible with the present data

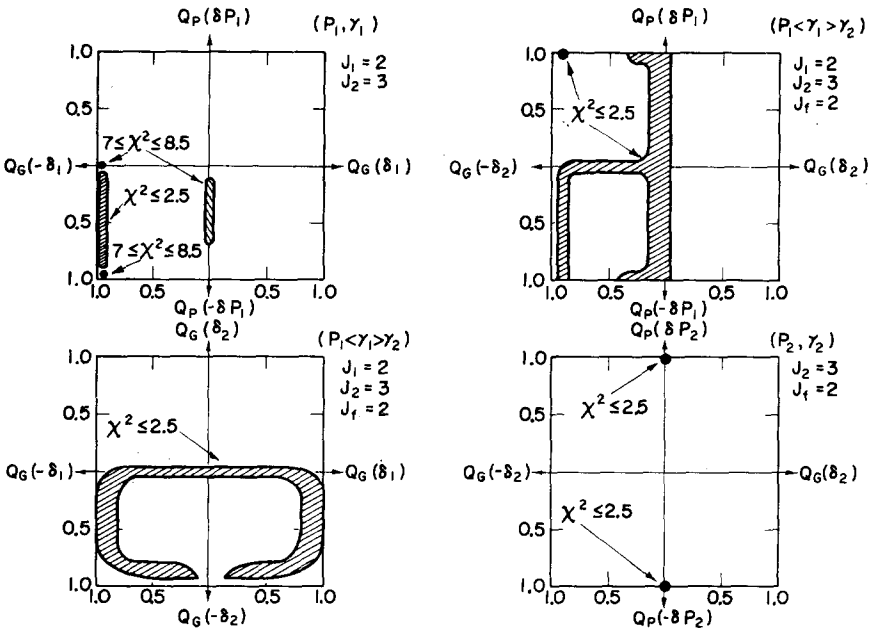


Fig. 8. A detailed summary of the $\chi^2$ analysis of the 1–2 and the 1–3 correlation data involving the 2.05 and 0.65 MeV levels for postulated spins of $J_1 = 2$ and $J_2 = 3$ for these respective levels. The subscripts on the symbols P and $\gamma$ are defined in fig. 2.

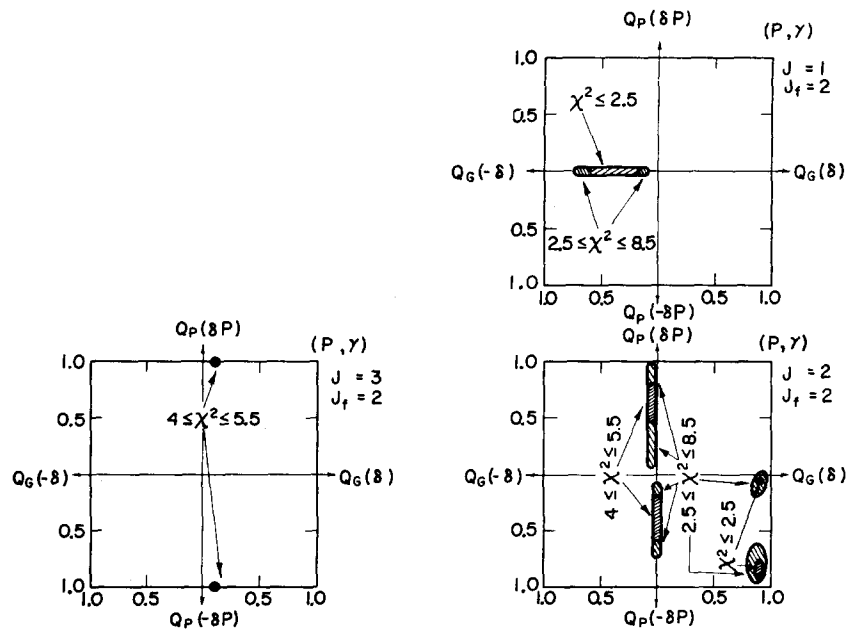


Fig. 9. A detailed summary of the $\chi^2$ analysis of the 1–2 correlation data for the 1.31 MeV level for postulated spins of $J = 1$, 2 and 3.

TABLE 3

Predicted values of the correlation coefficients associated with typical minima in the $\chi^2$ surface for the 2.05 and the 0.65 MeV levels

| | | Cascade [a] | | | | $p_1\langle\gamma_1\rangle\gamma_2$ | | | $p_1, \gamma_1$ | | | $p_2, \gamma_2$ | | | |
|---|---|---|---|---|---|---|---|---|---|---|---|---|---|---|---|
| | | [{Experimental results} {$A_2 = -0.215\pm0.03$} {$A_4 = -0.03\pm0.04$} | | | | | | | {$A_2 = -0.027\pm0.03$} {$A_4 = -0.09\pm0.04$} | | | {$A_2 = -0.33\pm0.025$} {$A_4 = 0.007\pm0.04$}] | | | |
| $J_1$ | $J_2$ | $Q_p(\delta P_1)$ | $Q_G(\delta_1)$[b] | $Q_G(\delta_2)$ | $Q_p(\delta P_2)$ | $A_2$ | $A_4$ | $\chi^2$ | $A_2$ | $A_4$ | $\chi^2$ | $A_2$ | $A_4$ | $\chi^2$ | $\Sigma\chi^2$ |
| 1 | 1 | 0 | 0.05(−) | 0.17(+) | 0 | 0.158 | 0 | 166 | −0.077 | 0 | 8 | −0.336 | 0 | 0.1 | 174.1 |
| | | 0 | 0.95(−) | 0.95(+) | 0 | −0.027 | 0 | 43 | −0.077 | 0 | 8 | −0.386 | 0 | 5 | 56 |
| 1 | 2 | 0 | 0 | 0.45(−) | 0 | −0.183 | 0 | 2 | −0.050 | 0 | 5 | −0.365 | 0 | 2 | 9 |
| | | 0 | 0 | 0.90(−) | 0.95(−) | −0.184 | 0 | 2 | −0.050 | 0 | 5 | −0.363 | 0.017 | 2 | 9 |
| 1 | 3 | 0 | 1 | 0 | 1 | −0.120 | 0 | 11 | 0.071 | 0 | 17 | −0.343 | 0 | 0.3 | 28.3 |
| | | 0 | 1 | 0.05(−) | 1 | −0.255 | 0 | 3 | 0.071 | 0 | 17 | −0.729 | 0.022 | 255 | 275 |
| 2 | 1 | 0.50(−) | 0.05(+) | 0.17(+) | 0 | −0.153 | 0 | 5 | 0.015 | −0.037 | 4 | −0.336 | 0 | 0.1 | 9.1 |
| | | 0.50(−) | 0.05(+) | 0.95(+) | 0 | −0.176 | 0 | 3 | 0.015 | −0.037 | 4 | −0.386 | 0 | 5 | 12 |
| 2 | 2 | 1 | 0.10(−) | 0.5 (−) | 0.90(−) | −0.192 | 0.047 | 5 | −0.004 | −0.016 | 4 | −0.359 | 0.047 | 2 | 11 |
| | | 0 | 0.10(−) | 0.90(−) | 0.95(−) | −0.158 | 0 | 5 | −0.003 | 0 | 6 | −0.363 | 0.017 | 2 | 13 |
| 2 | 3 | 0 | 0.95(−) | 0 | 1 | −0.069 | 0 | 19 | −0.038 | 0 | 5 | −0.343 | 0 | 0.3 | 24.5 |
| | | 0.20(−) | 0 | 0 | 1 | −0.180 | 0 | 2 | −0.075 | 0 | 8 | −0.343 | 0 | 0.3 | 10.3 |
| 3 | 1 | 1 | 1 | 0.17(+) | 0 | −0.230 | 0 | 1 | 0.490 | −0.299 | 344 | −0.336 | 0 | 0.1 | 345.1 |
| | | 1 | 1 | 0.95(+) | 0 | −0.265 | 0 | 4 | 0.490 | −0.299 | 344 | −0.386 | 0 | 5 | 353 |
| 3 | 2 | 1 | 0.50(+) | 0.45(−) | 0 | −0.224 | 0.010 | 1 | 0.829 | 0.225 | 932 | −0.365 | 0 | 2 | 935 |
| | | 1 | 0.50(+) | 0.90(−) | 0.95(−) | −0.226 | 0.019 | 2 | 0.829 | 0.225 | 932 | −0.363 | 0.017 | 2 | 936 |
| 3 | 3 | 1 | 0.20(−) | 0 | 1 | −0.228 | 0 | 1 | −0.045 | −0.060 | 1 | −0.343 | 0 | | 2.1 |
| | | 1 | 0.20(−) | 0.02(−) | 1 | −0.396 | 0.0003 | 40 | −0.045 | −0.060 | 1 | −0.597 | 0.009 | 114 | 155 |

[a]) Refer to the notation used in fig. 2.

[b]) The symbol in parentheses refers to the sign of the mixing ratio.

TABLE 4

Predicted values of the correlation coefficients associated with typical minima in the $\chi^2$ surface for the 1.31 MeV and the unresolved 0.99 and 1.06 MeV levels

| | | Cascade | | $P, \gamma$(1.31 MeV) | | | $P, \gamma$(0.99, 1.06 MeV) | | | | |
|---|---|---|---|---|---|---|---|---|---|---|---|
| | | [Experimental results | $A_2 = 0.199 \pm 0.034$ | $A_4 = 0.086 \pm 0.062$] | | | | $A_2 = 0.0004 \pm 0.013$ | $A_4 = -0.015 \pm 0.02$] | | |
| $J$ | $J_f$ | $Q_p(\delta P)$ | $Q_G(\delta)$ [a] | $A_2$ | $A_4$ | $\chi^2$ | $Q_p(\delta P)$ | $Q_G(\delta)$ | $A_2$ | $A_4$ | $\chi^2$ |
| 1 | 2 | 0 | 0.35(−) | 0.200 | 0 | 1.9 | 0 | 0.85(−) | 0.020 | 0 | 2.7 |
| | | 0 | 0.10(−) | 0.131 | 0 | 5.9 | 0 | 0.90(−) | −0.029 | 0 | 5.4 |
| 2 | 2 | 0.05(−) | 0.90(+) | 0.210 | 0.150 | 1.2 | 0 | 0.10(−) | −0.003 | 0 | 0.6 |
| | | 0.90(−) | 0.90(+) | 0.226 | 0.084 | 0.6 | 1 | 0.10(−) | −0.004 | −0.016 | 0.1 |
| 3 | 2 | 1 | 0.10(+) | 0.267 | 0.045 | 4.4 | 1 | 0 | −0.343 | 0 | 676 |
| | | 1 | 0.05(+) | 0.090 | 0.022 | 11.4 | 1 | 1 | 0.123 | 0.449 | 624 |

[a] The symbol in parentheses refers to the sign of the mixing ratio.

would be 2 and 3 for the 2.05 and the 0.65 MeV level, respectively. This particular spin sequence is of special interest because it agrees with the tentative assignment based on the n-γ experiment performed by Nadjakov [20]). In fig. 8 is a detailed presentation of the projections of the minima in the $\chi^2$ surface which define the most probable range of angular momentum mixing ratios $\delta$ which are compatible with this set of spins. Note that each of the four quadrants in the graphs correspond to one of the four possible sign combinations for the two relevant mixing ratios. It is unfortunate that for this particular spin sequence, the 1–3 correlation measurements did not place a very strong constraint on the mixing ratios.

In table 4 the corresponding results for the 1–2 correlations involving the 1.31 and the unresolved 0.99–1.06 MeV levels are presented. A detailed summary of the projected minima in the $\chi^2$ surface for the 1.31 MeV level is given in fig. 9, and it is apparent that it is impossible unambiguously to eliminate any of the three possible spin-values. The results for the unresolved 0.99–1.06 MeV levels, however, indicate that a spin of 3 is rather unlikely for either of these levels.

## 5. Discussion

The analysis of the experimental data in the search for a unique set of spin values for some of the low-lying states of $^{20}$F was based on the use of eq. (4.5). This tacit assumption that the plane-waves approximation is valid in the region near 180° is somewhat substantiated by the agreement, for the 0.65 MeV level, between the results obtained in this fashion and the results extracted by Chagnon [6]) using the distorted-wave Born approximation. These results are summarized in table 2. There is, however, a distinct discrepancy in the corresponding results for the 1.31 MeV level. Due to the fact that there was not enough available information to determine uniquely the distortion parameters used in Chagnon's analysis, it may be possible to find an alternate set of these parameters which could resolve this discrepancy. Although the results presented in table 4 for the 1.31 MeV level do not allow a unique spin assignment to be made with an adequate margin of certainty, the smallest $\chi^2$ values do occur for a spin of 2 which tends to confirm Chagnon's conclusion for this level. It is important to note that the distorted-wave analysis employed by Chagnon [6]) and the plane-wave analysis used in the present work are both based on the assumption that spin orbit corrections are negligible. The validity of this assumption for this particular reaction obviously requires further investigation.

Although the spins of the levels investigated could not be uniquely determined, it has been possible to put rather strong conditions on the relative intensities of the angular-momentum matrix elements associated with the relevant radiative transitions. A measurement of the linear polarization of the 0.65 MeV gamma radiation would probably remove much of the remaining ambiguity [8]).

It is of interest to note that the shell-model calculation by Dazai [2]) predicts a spin of 2 and 3 for the 2.05 and 0.65 MeV levels respectively. These predictions are com-

patible with the results obtained from the analysis of the present data. These results are also in agreement with the tentative spin sequence based on the n-$\gamma$ experiment by Nadjakov [20]).

The support and encouragement of this work by Professor M. L. Wiedenbeck is gratefully acknowledged. Special thanks are also due to Professor P. Chagnon for several valuable discussions and for providing a copy of his paper prior to publication. The author would also like to thank Mr. W. Greenberg for his assistance in writing the computer programs, and the following individuals for their assistance in running the accelerator and in processing the data: Mr. P. Auer, Mrs. C. Bennett, Mr. D. Donnelly, Mr. J. Henry, Mr. A. Miller and Mr. S. Samanders.

## Appendix

The correction for the finite solid angle subtended by the detectors was based on the method outlined by Rose [12]). The correlation attenuation factors for the 7.6 cm by 7.6 cm NaI(Tl) crystal were taken from the recent work of Herskind and Yoshizawa [21]) in which these factors were experimentally measured. However, the attenuation factors for the proton detector had to be calculated.

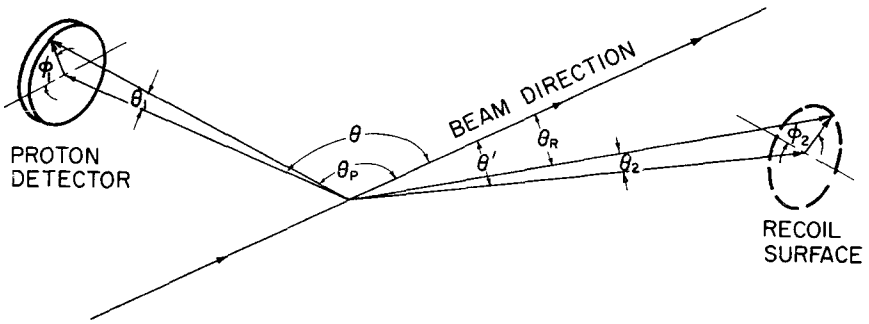


Fig. 10. A schematic diagram for defining the angular variables employed in making the correction for the finite solid angles subtended by the disc-shaped proton detector.

In the plane-wave approximation [14]), the d, p stripping reaction is analogous to a plane wave of neutrons incident on the target along the line defined by the recoiling nucleus. Calculation of the attenuation coefficient for the proton detector therefore involves integrating the relevant Legendre polynomials over the surface swept out by those recoiling nuclei associated with the detected protons. For the case in which the beam passes through an annular detector, the associated cylindrical symmetry makes the determination of the recoil surface and the subsequent integrations very easy. For the disc-shaped detector located at 135°, however, the recoil surface is distorted and its exact determination becomes rather involved. A schematic diagram of this latter case is shown in fig. 10.

The use of vector notation greatly simplifies the derivation of the essential equations. With this approach it is straightforward to show that

$$\cos\theta_p = (\cos\theta_1 \cos\theta - \sin\theta_1 \sin\theta \cos\varphi_1), \tag{A.1}$$

and that the corresponding equation involving the recoil direction is

$$\cos\theta_R = (\cos\theta_2 \cos\theta' + \sin\theta_2 \sin\theta' \cos\varphi_2), \tag{A.2}$$

where the recoil angles are defined as negative with respect to those for the proton detector. The angular notation is defined in fig. 10. The requirement that the three lines, defined by the incident deuteron beam direction, the proton direction and the direction of motion of the recoil nucleus, all lie in the same plane yields the following constraint equation:

$$\operatorname{tg}\theta_1 \sin\varphi_1(-\sin\theta' + \operatorname{tg}\theta_2 \cos\varphi_2 \cos\theta') = (\sin\theta + \operatorname{tg}\theta_1 \cos\varphi_1 \cos\theta)\operatorname{tg}\theta_2 \sin\varphi_2. \tag{A.3}$$

From eqs. (A.2) and (A.3), a quadratic equation in $\cos\theta_2$ can be obtained by eliminating the angle $\varphi_2$. Note that the angle to the centre of the proton detector $\theta$ is fixed at 135° and that the corresponding recoil angle $\theta'$ is determined from the kinematics of the reaction. With $\theta_1$ fixed at its maximum value, any given angle $\varphi_1$ defines a corresponding angle $\theta_p$ from eq. (A.1). From kinematics the corresponding $\theta_R$ is then determined. The equation obtained from eqs. (A.2) and (A.3) by eliminating $\varphi_2$ then determines the angle $\theta_2$. All solutions obtained in this manner were double-checked by requiring them to satisfy eqs. (A.1)–(A.3).

Using this approach, it was found that the maximum angle $\theta_2$, which is fixed by the perimeter of the recoil surface, did not deviate from an average constant value by more than half a degree. This variation of the maximum angle $\theta_2$ as a function of $\varphi_2$ was well approximated by the following expression, which was used by Yoshiki for a similar problem [22]):

$$\theta_2 \approx \gamma(1 + \eta \sin\varphi_2), \qquad 0 \leqq \varphi_2 \leqq \pi, \tag{A.4}$$

where $\gamma$ and $\eta$ are adjustable constants. Note that the recoil surface is symmetric about the line defined by the radius vector with $\varphi_2 = 0$ or $\varphi_2 = \pi$. With this approximation, the integration of the Legendre polynomials over the recoil surface can be expressed in closed form in terms of zero-order Bessel functions [22]).

## References

1) D. Kurath, Phys. Rev. **132** (1963) 1147
2) T. Dazai, Prog. Theor. Phys. **27** (1962) 433
3) V. M. Rout, W. M. Jones and D. G. Waters, Nuclear Physics **45** (1963) 369
4) M. E. O. De Lopéz, J. Richards and M. Mazari, Nuclear Physics **51** (1964) 321
5) A. Z. El-Behay *et al.*, Nuclear Physics **56** (1964) 224
6) P. Chagnon, Nuclear Physics **59** (1964) 257

7) R. H. Bassel, R. M. Drisko and G. R. Satchler, Oak Ridge National Laboratory Report ORNL-3240, unpublished
8) P. Chagnon, private communication
9) G. R. Satchler and W. Tobocman, Phys. Rev. **118** (1960) 1566
10) P. Chagnon, Rev. Sci. Instr. **32** (1961) 68
11) W. Whaling, Handbuch der Physik, Vol. 34 (Springer-Verlag, Berlin, 1958) p. 193
12) M. E. Rose, Phys. Rev. **91** (1953) 610
13) M. E. Rose, Oak Ridge National Laboratory Report ORNL-2516, unpublished
14) G. R. Satchler, Proc. Phys. Soc. **A66** (1953) 1081
15) M. Ferentz and N. Rosenzweig, Argonne National Laboratory Report ANL-5324, unpublished
16) A. Simon, J. H. Vander Sluis and L. C. Biedenharn, Oak Ridge National Laboratory Report ORNL-1679, unpublished
17) E. Freiberg and V. Soergel, Z. Phys. **162** (1961) 114
18) V. M. Lobashev and V. A. Nazarenko, JETP **42** (1962) 370
19) R. W. Newsome, Jr. and H. J. Fishbeck, Phys. Rev. **133** (1964) B273
20) E. G. Nadjakov, Nuclear Physics **48** (1963) 492
21) B. Herskind and Y. Yoshizawa, Nucl. Instr. **27** (1964) 104
22) H. Yoshiki, Phys. Rev. **117** (1960) 773